Microsyst Technol (2017) 23:5079–5091
DOI 10.1007/s00542-017-3345-5

TECHNICAL PAPER

Buckling analysis of CNT-reinforced beams with arbitrary boundary conditions

A. M. Fattahi[1] · **Babak Safaei**[1]

Received: 11 December 2016 / Accepted: 27 February 2017 / Published online: 3 March 2017

Abstract Axial buckling characteristics of nanocomposite beams reinforced by single-walled carbon nanotubes (SWCNTs) are investigated. Various types of beam theories namely as Euler–Bernoulli beam theory, Timoshenko beam theory and Reddy beam theory are used to analyze the buckling behavior of carbon nanotube-reinforced composite beams. Generalized differential quadrature (GDQ) method is utilized to discretize the governing differential equations along with four commonly used boundary conditions. The material properties of the nanocomposite beams are obtained using molecular dynamic (MD) simulation corresponding to both of short-(10,10) SWCNT and long-(10,10) SWCNT composites which are embedded by amorphous polyethylene matrix. Then the results obtained directly from MD simulations are matched with those calculated by the rule of mixture to extract appropriate values of carbon nanotube efficiency parameters accounting for the scale-dependent material properties. Selected numerical results are presented to indicate the influences of nanotube volume fraction and end supports on the critical axial buckling loads of nanoconposite beams relevant to long- and short-nanotube composites.

✉ A. M. Fattahi
a.fattahi@iaut.ac.ir

[1] Department of Mechanical Engineering, Tabriz Branch, Islamic Azad University, Tabriz, Iran

1 Introduction

The discovery of carbon nanotubes by Iijima (1991) has inspired the promise of a new generation in diverse engineering, materials science, and reinforced composite structures due to superior mechanical and physical properties of carbon nanotubes over any other known materials. One of the most useful applications of this new material is the use of it as strong, light-weight and high-toughness fibers for nanocomposite structures. A large number of theoretical and experimental researches using carbon nanotubes as reinforcing fibers have been carried out.

Liao and Li (2001) carried molecular mechanics simulations to study the interfacial characteristics of polystyrene-nanotube interface. They noted that on relaxing the structure without applying any external force or displacement, there is a slight decrease in the nanotube diameter. Wei et al. (2001) discussed the effect of chemical bonding between the carbon nanotube and polymer on effective load transfer in the composites. They observed better load transfer in case of double site bonding and higher shear strain. The load transfer properties between carbon nanotubes and polymer using theoretical models were studied by Lau (2003). They found that the maximum shear stress for pullout of a single-walled carbon nanotube (SWCNT) is comparatively higher than that for a multi-walled carbon nanotube. Hammel et al. (2004) focused on production and improvement of vapour grown carbon fibers for composite applications. Han and Elliot (2007) presented classical molecular dynamics (MD) simulations of model polymer/carbon nanotube composites constructed by embedding an armchair SWCNT into methyl methacrylate polymer matrix. By comparing the simulation results with the macroscopic rule of mixture for composite systems, they showed that for strong interfacial interactions, there

can be large deviations of the results from the rule of mixture.

There so many other researches in which the response of nanocomposite structures subjected to various loading conditions have been studied with computational techniques and simulation models (Zeng et al. 2008; Xiao et al. 2006; Esawi and Farag 2007; Lau et al. 2006; Shokrieh and Rafiee 2010; Qian et al. 2000; Haque and Ramasetty 2005; Saffar et al. 2008; Frankland et al. 2003; Villoria and Miravete 2007; Cao et al. 2010).

Continuing with the experimental investigations, Schadler et al. (Schadler et al. 1998) dispersed 5% by weight of multi-walled carbon nanotubes in an epoxy resin and cured the mixture using a hardener. The results indicated that the composite showed a marked difference between the change of properties in tension and compression due to the multi-walled carbon nanotube addition. Epoxy nanocomposites of different content of carbon nanofibers were fabricated and studied in terms of mechanical and electrical properties by Bal (2010). He found that flexural modulus and hardness increase significantly in refrigerated samples due to prevention of aggregates of nanofibers. On the basis of various testing procedures, it has been shown an improvement in stiffness of the carbon nanotube-polymer composite of up to 20–40% (Qian et al. 2000; Gong et al. 2000; Xu et al. 2002) and 200–350% (Geng et al. 2002; Cadek et al. 2002; Lozano and Barrera 2001), by addition of carbon nanotubes.

According to the above literature review, it can be concluded that carbon nanotubes are envisaged to be ideal reinforcements for composite materials with different polymers. However, Polyethylene is the simplest and the least expensive of all the polymers available. The molecular structure of polyethylene is the easiest to generate through no functional units and just one repetitive unit. At the atomic level, polyethylene is classified as amorphous polyethylene and crystalline polyethylene. In amorphous case, the structure of each monomer unit remains the same, but adjacent units are rotated around the connecting C–C bond. This type of structure leads to the same properties in all the directions.

In the current study, buckling behavior of nanocomposite beams which are reinforced by (10,10) armchair SWCNTs embedded in amorphous polyethylene is investigated based on the various elastic beam theories (Labuschange et al. 2009). Generalized differential quadrature (GDQ) method is utilized to discretize the governing differential equations along with four sets of end supported namely as simply supported-simply supported, clamped–clamped, clamped-simply supported, and clamped-free. Then the material properties calculated by the beam theories in conjunction with the rule of mixture are fitted with those obtained directly from MD simulations to extract consistent values of carbon nanotube efficiency parameters accounting for the scale-dependent material properties corresponding to both of short and long carbon nanotube reinforcements.

2 Overview of different beam theories

There are various beam theories to describe the behavior of beams. Consider a straight uniform beam with the length L and rectangular cross-section of thickness h. A coordinate system (x, y, z) is introduced on the central axis of the beam, whereas the x axis is taken along the length of the beam, the y axis in the width direction and the z axis is taken along the depth (height) direction. Also, the origin of the coordinate system is selected at the left end of the beam. It is assumed that the deformations of the beam take place in the x–z plane, so the displacement components (u_1, u_2, u_3) along the axis (x, y, z) are only dependent on the x and z coordinates and time t. In a general form, the following displacement field can be written:

$$u_1(x,z,t) = -z\frac{\partial w(x,t)}{\partial x} + \psi(z)\left(\frac{\partial w(x,t)}{\partial x} + \varphi(x,t)\right)$$

$$u_2(x,z,t) = 0 \tag{1}$$

$$u_3(x,z,t) = w(x,t)$$

where w and φ are the transverse displacement and angular displacement of the beam, respectively, and $\psi(z)$ is the shape function as follows:

For Euler–Bernoulli beam theory (EBT): $\psi(z) = 0$.
For Timoshenko beam theory (TBT): $\psi(z) = z$.
For Reddy beam theory (RBT): $\psi(z) = z - \frac{4z^3}{3h^2}$.

3 Buckling analysis of nanocomposite beams

3.1 Constitutive equations

The stress-displacement and Euler–Lagrange relations for each type of beam theory can be expressed as

For Euler–Bernoulli beam theory:

$$\varepsilon_{xx} = \frac{\partial u_1}{\partial x} = -z\frac{\partial^2 w}{\partial x^2} \rightarrow \sigma_{xx} = \frac{-zE_{11}}{1-\nu^2}\frac{\partial^2 w}{\partial x^2} \tag{2-a}$$

$$\gamma_{xz} = \frac{\partial u_1}{\partial z} + \frac{\partial u_3}{\partial x} = 0 \rightarrow \sigma_{xz} = 0 \tag{2-b}$$

$$\frac{\partial^2 M}{\partial x^2} - P\frac{\partial^2 w}{\partial x^2} = 0 \tag{3}$$

For Timoshenko beam theory:

$$\varepsilon_{xx} = \frac{\partial u_1}{\partial x} = z\frac{\partial \varphi}{\partial x} \rightarrow \sigma_{xx} = \frac{zE_{11}}{1-\nu^2}\frac{\partial \varphi}{\partial x} \tag{4-a}$$

$$\gamma_{xz} = \frac{\partial u_1}{\partial z} + \frac{\partial u_3}{\partial x} = \frac{\partial w}{\partial x} + \varphi \rightarrow \sigma_{xz} = G_{12}\left(\frac{\partial w}{\partial x} + \varphi\right) \tag{4-b}$$

$$\frac{\partial Q}{\partial x} - P\frac{\partial^2 w}{\partial x^2} = 0 \tag{5-a}$$

$$\frac{\partial M}{\partial x} - Q = 0 \tag{5-b}$$

For Reddy beam theory:

$$\begin{aligned}\varepsilon_{xx} = \frac{\partial u_1}{\partial x} &= z\frac{\partial \varphi}{\partial x} - \frac{4z^3}{3h^2}\left(\frac{\partial \varphi}{\partial x} + \frac{\partial^2 w}{\partial x^2}\right) \rightarrow \sigma_{xx} \\ &= \frac{zE_{11}}{1-\nu^2}\frac{\partial \varphi}{\partial x} - \frac{4z^3E_{11}}{3h^3(1-\nu^2)}\left(\frac{\partial \varphi}{\partial x} + \frac{\partial^2 w}{\partial x^2}\right)\end{aligned} \tag{6-a}$$

$$\begin{aligned}\gamma_{xz} = \frac{\partial u_1}{\partial z} + \frac{\partial u_3}{\partial x} &= \left(1 - \frac{4z^2}{h^2}\right)\left(\varphi + \frac{\partial w}{\partial x}\right) \rightarrow \sigma_{xz} \\ &= G_{12}\left(1 - \frac{4z^2}{h^2}\right)\left(\varphi + \frac{\partial w}{\partial x}\right)\end{aligned} \tag{6-b}$$

$$\frac{4}{3h^2}\frac{\partial^2 R}{\partial x^2} + \frac{\partial Q}{\partial x} - \frac{4}{h^2}\frac{\partial S}{\partial x} - P\frac{\partial^2 w}{\partial x^2} = 0 \tag{7-a}$$

$$\frac{\partial M}{\partial x} - \frac{4}{3h^2}\frac{\partial R}{\partial x} - Q + \frac{4}{h^2}S = 0 \tag{7-b}$$

where

$$M = \int z\sigma_{xx}dA$$

$$Q = \int \sigma_{xz}dA$$

$$R = \int z^3\sigma_{xx}dA$$

$$S = \int z^2\sigma_{xz}dA$$

and P is the critical buckling load.

By substituting stress-displacement relations into the respective Euler–Lagrange relations, the constitutive equations corresponding to each type of beam theory can be obtained as

For Euler–Bernoulli beam theory:

$$\frac{E_{11}I}{1-\nu^2}\frac{\partial^4 w}{\partial x^4} - P\frac{\partial^2 w}{\partial x^2} = 0 \tag{8}$$

For Timoshenko beam theory:

$$(\kappa G_{12}A - P)\frac{\partial^2 w}{\partial x^2} + \kappa G_{12}A\frac{\partial \varphi}{\partial x} = 0 \tag{9-a}$$

$$-\kappa G_{12}A\frac{\partial w}{\partial x} + \frac{E_{11}I}{1-\nu^2}\frac{\partial^2 \varphi}{\partial x^2} - \kappa G_{12}A\varphi = 0 \tag{9-b}$$

For Reddy beam theory:

$$\begin{aligned}&\frac{E_{11}I}{21(1-\nu^2)}\frac{\partial^4 w}{\partial x^4} + \left(\frac{8G_{12}A}{15} - P\right)\frac{\partial^2 w}{\partial x^2} \\ &\quad + \frac{16E_{11}I}{105(1-\nu^2)}\frac{\partial^3 \varphi}{\partial x^3} + \frac{8G_{12}A}{15}\frac{\partial \varphi}{\partial x} = 0\end{aligned} \tag{10-a}$$

$$\begin{aligned}&-\frac{16E_{11}I}{105(1-\nu^2)}\frac{\partial^3 w}{\partial x^3} - \frac{8G_{12}A}{15}\frac{\partial w}{\partial x} \\ &\quad + \frac{68E_{11}I}{105(1-\nu^2)}\frac{\partial^2 \varphi}{\partial x^2} - \frac{8G_{12}A}{15}\varphi = 0\end{aligned} \tag{10-b}$$

where A, I are the cross-sectional area and moment of inertia of the beam, respectively, and κ is the shear correction factor.

3.2 Rule of mixture

In the present work, it is assumed that the carbon nanotube-reinforced composite is made of a mixture of (10,10) armchair SWCNT and polyethylene matrix with isotropic behavior. It has been shown that carbon nanotube-reinforced composites have anisotropic material properties (Han and Elliott 2007; Zhang and Shen 2006). On the basis of the rule of mixture, the effective values of Young's modulus and shear modulus of carbon-nanotube-reinforced composite can be evaluated as (Shen 2009)

$$E_{11} = \vartheta_1 V_{CNT}E_{11}^{CNT} + V_m E^m \tag{11-a}$$

$$\frac{\vartheta_2}{E_{22}} = \frac{V_{CNT}}{E_{22}^{CNT}} + \frac{V_m}{E^m} \tag{11-b}$$

$$\frac{\vartheta_3}{G_{12}} = \frac{V_{CNT}}{G_{12}^{CNT}} + \frac{V_m}{G^m} \tag{11-c}$$

in which $E_{11}^{CNT}, E_{22}^{CNT}, G_{12}^{CNT}$ are longitudinal Young's modulus, transverse Young's modulus, and shear modulus of the carbon nanotube, respectively; E^m, G^m are Young's modulus and shear modulus of the isotropic matrix, respectively; V_{CNT}, V_m are the volume fractions of carbon nanotube and matrix, respectively and are related by

$$V_{CNT} + V_m = 1 \tag{12}$$

The coefficients of $\vartheta_1, \vartheta_2, \vartheta_3$ are the carbon nanotube efficiency parameters to incorporate the scale-dependent characteristic of material properties which are determined with the results obtained directly from MD simulations.

4 Generalized differential quadrature method

The GDQ method is one of the most efficient numerical techniques to solve various boundary value problems. Many researchers have recently suggested the application of the generalized differential quadrature (GDQ) method to the analysis of nanostructures (Haftchenari et al. 2007; Malekzadeh and Fiouz 2007; De Rosa et al. 2008; Hu et al. 2009; Sepahi et al. 2010; Pradhan and Murmu 2010). This method has shown superb accuracy, efficiency, convenience and great potential in solving complicated partial differential equations. The basic idea of the differential quadrature method lies in the approximation of partial derivative of a function with respect to a coordinate at a discrete point as a weighted linear sum of the function values at all discrete points along that coordinate direction. Let $\frac{\partial^r f}{\partial x^r}$ be the rth derivative of a function $f(x)$ which can be expressed as a linear sum of the function values

$$\left.\frac{\partial^r f(x)}{\partial x^r}\right|_{x=x_P} = \sum_{Q=1}^{n} A_{PQ}^{(r)} f(x_P) \tag{13}$$

where n is the number of total discrete grid points used in the approximation process and $A_{PQ}^{(r)}$ are weighting coefficients. The weighting coefficients of the first derivative are determined by

$$A_{PQ}^{(1)} = \frac{M(x_P)}{(x_P - x_Q)M(x_Q)} (P, Q = 1, 2, \ldots, n; P \neq Q) \tag{14}$$

where

$$M(x_P) = \prod_{Q=1; Q\neq P}^{n} (x_P - x_Q) \tag{15}$$

The weighting coefficients of higher-order derivatives can be obtained through the following recurrence relation

$$A_{PQ}^{(r)} = \begin{cases} r\left[A_{PQ}^{(r-1)} A_{PQ}^{(1)} - \frac{A_{PQ}^{(r-1)}}{x_p - x_q}\right], & P \neq Q \\ -\sum\limits_{Q=1}^{n} A_{PQ}^{(r)}, & P = Q \ (P, Q = 1, 2, \ldots, n; 2 \leq r \leq n-1) \end{cases} \tag{16}$$

4.1 Implementation of GDQ method into the constitutive equations

By applying the GDQ method, the discrete counterparts of constitutive differential equations corresponding to each type of beam theory at the rth given point can be expressed as

For Euler–Bernoulli beam theory:

$$\frac{E_{11} I}{(1-\nu^2)} \sum_{s=1}^{n} A_{rs}^{(4)} W_s - P \sum_{s=1}^{n} A_{rs}^{(2)} W_s = 0 \tag{17}$$

For Timoshenko beam theory:

$$(\kappa G_{12} A - P) \sum_{s=1}^{n} A_{rs}^{(2)} W_s + \kappa G_{12} A \sum_{s=1}^{n} A_{rs}^{(1)} \phi_s = 0 \tag{18-a}$$

$$-\kappa G_{12} A \sum_{s=1}^{n} A_{rs}^{(1)} W_s + \frac{E_{11} I}{(1-\nu^2)} \sum_{s=1}^{n} A_{rs}^{(2)} \phi_s - \kappa G_{12} A \phi_r = 0 \tag{18-b}$$

For Reddy beam theory:

$$\begin{aligned} &\left(\frac{8 G_{12} A}{15} - P\right) \sum_{s=1}^{n} A_{rs}^{(2)} W_s \\ &\quad + \frac{16 E_{11} I}{105(1-\nu^2)} \sum_{s=1}^{n} A_{rs}^{(3)} \phi_s \\ &\quad + \frac{8 G_{12} A}{15} \sum_{s=1}^{n} A_{rs}^{(1)} \phi_s = 0 \end{aligned} \tag{19-a}$$

$$\begin{aligned} &- \frac{16 E_{11} I}{105(1-\nu^2)} \sum_{s=1}^{n} A_{rs}^{(3)} W_s - \frac{8 G_{12} A}{15} \sum_{s=1}^{n} A_{rs}^{(1)} W_s \\ &\quad + \frac{16 E_{11} I}{105(1-\nu^2)} \sum_{s=1}^{n} A_{rs}^{(2)} \phi_s - \frac{8 G_{12} A}{15} \phi_r = 0 \end{aligned} \tag{19-b}$$

4.2 Implementation of GDQ method into boundary conditions

Using the GDQ approximation, the discretized counterparts of different boundary conditions at the rth given point become for each type of beam theory as

For Euler–Bernoulli beam theory:

- Simply supported-simply supported:

$$W_r = 0, \sum_{s=1}^{n} A_{rs}^{(2)} W_s = 0 \quad \text{at edges } x = 0, L$$

- Clamped–clamped:

$$W_r = 0, \sum_{s=1}^{n} A_{rs}^{(1)} W_s = 0 \quad \text{at edges } x = 0, L$$

- Clamped-simply supported:

$$W_r = 0, \sum_{s=1}^{n} A_{rs}^{(1)} W_s = 0 \quad \text{at edge } x = 0$$

$$W_r = 0, \sum_{s=1}^{n} A_{rs}^{(2)} W_s = 0 \quad \text{at edge } x = L$$

- Clamped-free:

$$W_r = 0, \sum_{s=1}^{n} A_{rs}^{(1)} W_s = 0 \quad \text{at edge } x = 0$$

$$\sum_{s=1}^{n} A_{rs}^{(2)} W_s = 0, \sum_{s=1}^{n} A_{rs}^{(3)} W_s = 0 \quad \text{at edge } x = L$$

For Timoshenko beam theory:

- Simply supported-simply supported:

$$W_r = 0, \sum_{s=1}^{n} A_{rs}^{(1)} \phi_s = 0 \quad \text{at edges } x = 0, L$$

- Clamped–clamped:

$$W_r = 0, \phi_r = 0 \quad \text{at edges } x = 0, L$$

- Clamped-simply supported:

$$W_r = 0, \phi_r = 0 \quad \text{at edge } x = 0$$

$$W_r = 0, \sum_{s=1}^{n} A_{rs}^{(1)} \phi_s = 0 \quad \text{at edges } x = 0, L$$

- Clamped-free

$$W_r = 0, \phi_r = 0 \quad \text{at edge } x = 0$$

$$\sum_{s=1}^{n} A_{rs}^{(1)} \phi_s = 0, \phi_r + \sum_{s=1}^{n} A_{rs}^{(1)} W_s = 0 \quad \text{at edge } x = L$$

For Reddy beam theory:

- Simply supported-simply supported:

$$W_r = 0, \frac{68}{105} \sum_{s=1}^{n} A_{rs}^{(1)} \phi_s - \frac{16}{105} \sum_{s=1}^{n} A_{rs}^{(2)} W_s = 0 \quad \text{at edges } x = 0, L$$

- Clamped–clamped:

$$W_r = 0, \phi_r = 0 \quad \text{at edges } x = 0, L$$

- Clamped-Simply supported:

$$W_r = 0, \phi_r = 0 \quad \text{at edge } x = 0$$

$$W_r = 0, \frac{68}{105} \sum_{s=1}^{n} A_{rs}^{(1)} \phi_s - \frac{16}{105} \sum_{s=1}^{n} A_{rs}^{(2)} W_s = 0 \quad \text{at edge } x = 0$$

- Clamped-free:

$$W_r = 0, \phi_r = 0 \quad \text{at edge } x = 0$$

$$\frac{68}{105} \sum_{s=1}^{n} A_{rs}^{(1)} \phi_s - \frac{16}{105} \sum_{s=1}^{n} A_{rs}^{(2)} W_s = 0, \phi_r + \sum_{s=1}^{n} A_{rs}^{(1)} W_s = 0 \quad \text{at edges } x = L$$

5 Molecular dynamics simulation

The application of MD simulation considers as one of the most accurate methods to describe an atomic system which has the capability to handle simulations involving large numbers of atoms, allowing more complicated dynamic systems to be modeled in an approximately short period of time when compared with ab initio methods. Hanasaki et al. (2004) conducted a MD simulation of the molecular flow inside a modeled carbon nanotube junction as a strong gravitational field and periodic boundary conditions were applied in the flow direction. MD simulations of model polymer/carbon nanotube composites with different volume fraction were presented by Han and Elliott (2007). The simulation results supported the idea that it is possible to use carbon nanotubes to

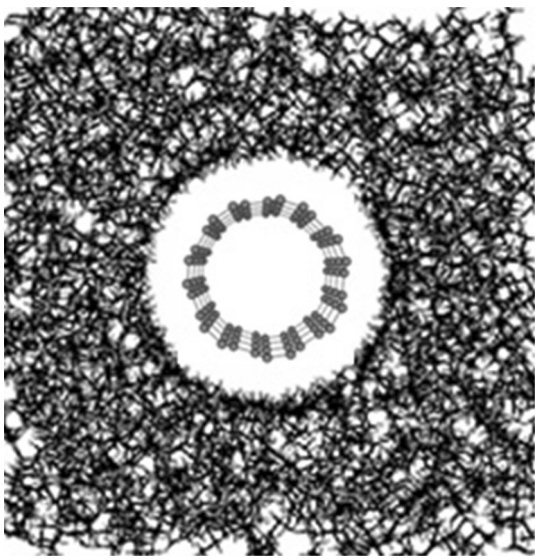

Fig. 1 (10,10) SWCNT embedded in an amorphous Polyethylene

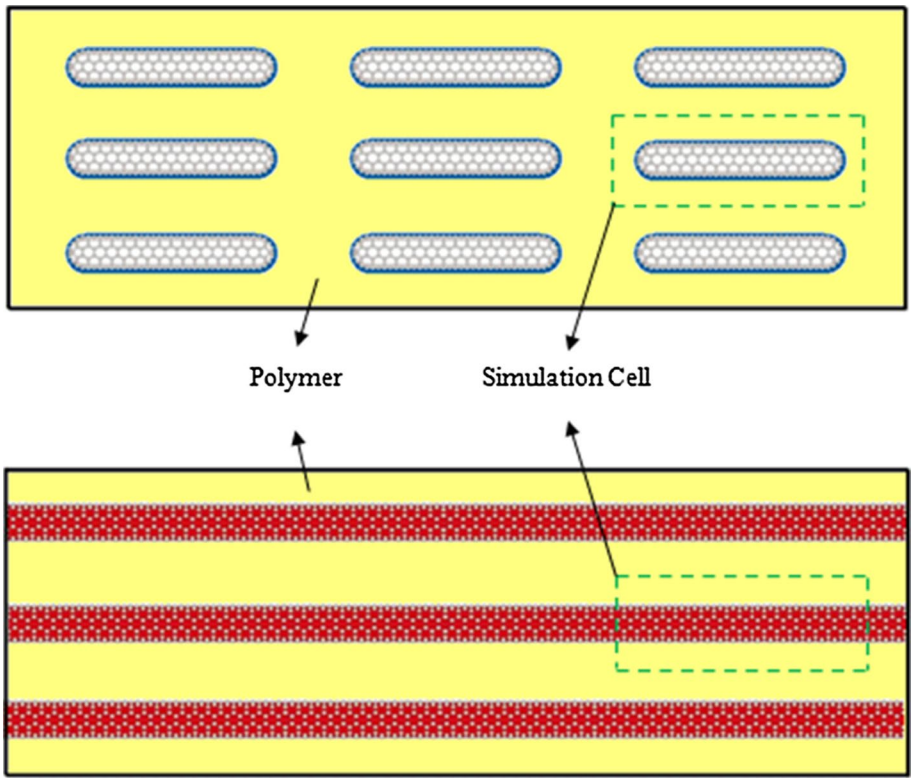

Fig. 2 Schematic MD simulation cell for both of short-SWCNT and long-SWCNT composites

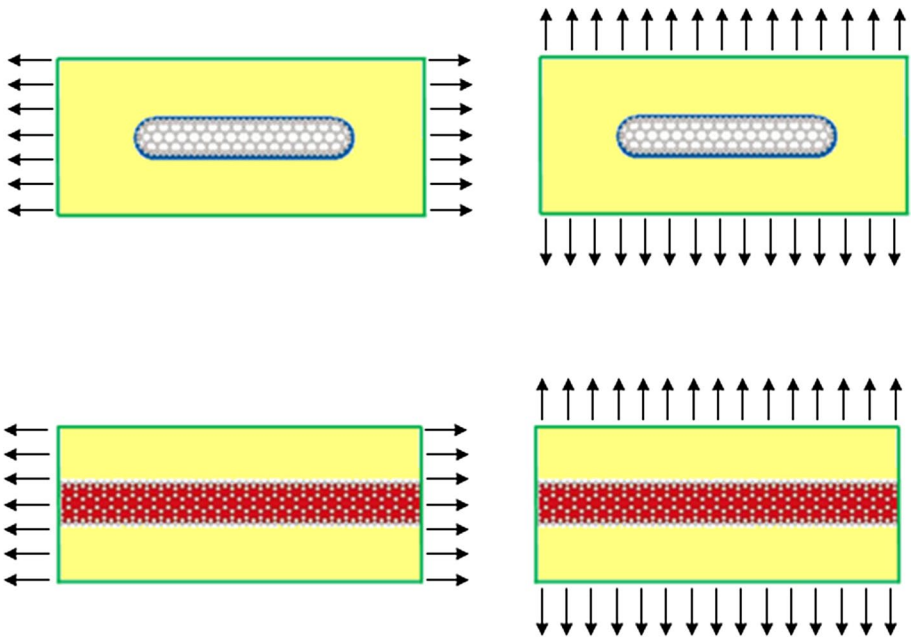

Fig. 3 Applied longitudinal and transverse strains to the MD simulation cell

mechanically reinforce an appropriate polymer matrix, especially in the longitudinal direction of the nanotube. Bi et al. (2006) studied the thermal conductivity of SWCNTs dependent on tube length and temperature based on MD simulation. They demonstrated that the vacancy scattering on phonons is stronger than the isotropic atom which causes more reduction on lattice thermal conductivity of carbon nanotubes.

In the current study, unidirectional carbon nanotube-polymer nanocomposites are simulated using the molecular dynamics simulator "NanoHive" (Nanorex Inc. 2005). NanoHive is a free open source MD simulator which has certain features that can be used to model different loading conditions of nanostructures (Nanorex Inc. 2005). Two types of composites are considered namely as long-(10,10) SWCNT composite and short-(10,10)

Table 1 MD results for elastic moduli of carbon nanotube-reinforced composites

Carbon nanotube volume fraction	Short-carbon nanotube composite		Long-carbon nanotube composite	
	Longitudinal modulus (GPa)	Transverse modulus (GPa)	Longitudinal modulus (GPa)	Transverse modulus (GPa)
(10,10) armchair nanotube ($D_{CNT} = 1.34$ nm)				
0%	3.22	3.22	3.22	3.22
5%	3.82	3.45	67.79	3.93
10%	5.56	4.44	101.02	5.10
15%	8.39	6.38	154.55	7.38
25%	13.51	7.27	250.38	8.46
(8,8) armchair nanotube ($D_{CNT} = 1.07$ nm)				
0%	3.22	3.22	3.22	3.22
5%	3.90	3.53	69.28	4.02
10%	5.68	4.54	103.24	5.21
15%	8.57	6.52	157.95	7.54
25%	13.81	7.43	255.88	8.65
(6,6) armchair nanotube ($D_{CNT} = 0.80$ nm)				
0%	3.22	3.22	3.22	3.22
5%	3.93	3.55	69.78	4.05
10%	5.72	4.57	103.99	5.25
15%	8.64	6.57	159.08	7.60
25%	13.90	7.48	257.73	8.71
(5,5) armchair nanotube ($D_{CNT} = 0.67$ nm)				
0%	3.22	3.22	3.22	3.22
5%	4.08	3.69	72.49	4.20
10%	5.94	4.75	108.03	5.45
15%	8.97	6.82	165.26	7.89
25%	14.45	7.77	267.73	9.04
(17,0) zigzag nanotube ($D_{CNT} = 1.32$ nm)				
0%	3.22	3.22	3.22	3.22
5%	3.66	3.36	61.01	3.71
10%	5.34	4.33	90.89	4.82
15%	8.05	6.21	139.06	6.97
25%	12.96	7.09	225.29	7.99
(14,0) zigzag nanotube ($D_{CNT} = 1.08$ nm)				
0%	3.22	3.22	3.22	3.22
5%	3.74	3.44	62.34	3.80
10%	5.45	4.43	92.89	4.92
15%	8.22	6.36	142.12	7.12
25%	13.25	7.24	225.29	8.17
(10,0) zigzag nanotube ($D_{CNT} = 0.78$ nm)				
0%	3.22	3.22	3.22	3.22
5%	3.77	3.46	62.77	3.83
10%	5.48	4.45	93.56	4.96
15%	8.29	6.40	143.12	7.18
25%	13.33	7.29	231.85	8.23
(8,0) zigzag nanotube ($D_{CNT} = 0.63$ nm)				
0%	3.22	3.22	3.22	3.22
5%	3.91	3.59	65.19	3.96
10%	5.70	4.63	97.15	5.14
15%	8.61	6.64	148.62	7.45
25%	13.86	7.56	240.78	8.54
	0.9595	0.975	0.9575	0.945

Table 2 Proper values of carbon nanotube efficiency parameters

Carbon nanotube volume fraction	ϑ_1	ϑ_2
Short-carbon nanotube reinforcement		
5%	0.0254	1.0351
10%	0.0443	1.2854
15%	0.0628	1.7798
25%	0.0740	1.8751
Long-carbon nanotube reinforcement		
5%	2.1577	1.1767
10%	1.6354	1.4765
15%	1.6868	2.0588
25%	1.6531	2.1820

SWCNT composite that both of them are surrounded by amorphous polyethylene matrix (Fig. 1). As shown in Fig. 2, a simulation cell with approximate dimensions of $5 \times 5 \times 10$ nm is utilized for all simulations which are established using the adaptive intermolecular reactive empirical bond order (AIREBO) potential (Stuart et al. 2000). The AIREBO potential is an extension of the commonly used REBO potential developed for solid carbon and hydrocarbon molecules (Stuart et al. 2000). It includes the covalent bonding interactions represented by REBO potential together with the Lennard-Jones terms and torsional interactions as

$$U^{AIREBO} = \frac{1}{2}\sum_{i}\sum_{j\neq i}\left(U_{ij}^{REBO} + U_{ij}^{LJ} + \sum_{k\neq i,j}\sum_{p\neq i,j,k} U_{kijp}^{Torsional}\right) \quad (20)$$

The MD simulations presented here are all performed at constant temperature equal to the room temperature (300 K). The van Gunstern-Berendsen thermostat (Berendsen et al. 1984) is implemented in such a way that the scaling factor is used after each step of the MD simulation; the velocities of the atoms of system are scaled as the average kinetic energy remains approximately constant. A time step of 0.5*fs* is selected with about 2000 numbers of steps to simulate deformations of the MD cell under longitudinal and transverse strain.

Longitudinal and transverse strains are applied to the MD cell, respectively, by mathematically changing the coordinates of the atoms to an extended strained condition as depicted in Fig. 3. Then, using the NanoHive simulator, various time steps to relax the system of atoms to their equilibrium position are set up to enable the MD cell reaches to the equilibrium configuration. This procedure is repeated for different values of the tensile strain while for 5% value of the strain. The stress–strain curves of the MD cells are obtained which result in the values of Young's modulus in the longitudinal and transverse directions. The values of Young's modulus obtained directly from the MD simulations are given in Table 1 corresponding to both of longitudinal and transverse directions and different values of carbon nanotube volume fraction.

6 Numerical results and discussion

The values of critical buckling load of (10,10) carbon nanotube-reinforced composite beams with four commonly used end supports are presented in this section corresponding to

Table 3 Critical buckling load of nanocomposite beam reinforced by short-SWCNT with simply supported-simply supported boundary conditions ($10^6 N$)

Aspect ratio (L/h)	Carbon nanotube volume fraction (%)	Euler–Bernoulli beam theory	Timoshenko beam theory	Reddy beam theory
10	0	0.2910	0.2830	0.2830
	5	0.3440	0.3337	0.3337
	10	0.4990	0.4822	0.4822
	15	0.7504	0.7241	0.7241
	25	1.2003	1.1427	1.1428
20	0	0.0728	0.0719	0.0722
	5	0.0860	0.0853	0.0853
	10	0.1247	0.1237	0.1237
	15	0.1876	0.1859	0.1859
	25	0.3001	0.2963	0.2963
50	0	0.0116	0.0116	0.0116
	5	0.0138	0.0137	0.0137
	10	0.0200	0.0199	0.0199
	15	0.0300	0.0300	0.0300
	25	0.0480	0.0479	0.0479

Table 4 Critical buckling load of nanocomposite beam reinforced by short-SWCNT with clamped–clamped boundary conditions ($10^6 N$)

Aspect ratio (L/h)	Carbon nanotube volume fraction (%)	Euler–Bernoulli beam theory	Timoshenko beam theory	Reddy beam theory
10	0	1.1407	1.1096	1.1096
	5	1.3485	1.3084	1.3084
	10	1.9561	1.8907	1.8907
	15	2.9415	2.8392	2.8393
	25	4.7052	4.4805	4.4807
20	0	0.2928	0.2881	0.2881
	5	0.3431	0.3403	0.3403
	10	0.4975	0.4936	0.4936
	15	0.7485	0.7417	0.7417
	25	1.1974	1.1822	1.1823
50	0	0.0464	0.0463	0.0463
	5	0.0552	0.0548	0.0548
	10	0.0799	0.0795	0.0795
	15	0.1201	0.1199	0.1199
	25	0.1919	0.1915	0.1915

Table 5 Critical buckling load of nanocomposite beam reinforced by short-SWCNT with clamped-simply supported boundary conditions ($10^6 N$)

Aspect ratio (L/h)	Carbon nanotube volume fraction (%)	Euler–Bernoulli beam theory	Timoshenko beam theory	Reddy beam theory
10	0	0.5834	0.5674	0.5674
	5	0.6897	0.6691	0.6691
	10	1.0005	0.9668	0.9668
	15	1.5045	1.4518	1.4518
	25	2.4066	2.2911	2.2910
20	0	0.1501	0.1476	0.1476
	5	0.1758	0.1744	0.1744
	10	0.2550	0.2529	0.2529
	15	0.3836	0.3802	0.3802
	25	0.6137	0.6059	0.6059
50	0	0.0239	0.0237	0.0237
	5	0.0282	0.0280	0.0280
	10	0.0409	0.0407	0.0407
	15	0.0614	0.0613	0.0613
	25	0.0982	0.0980	0.0980

different types of beam theory and carbon nanotube volume fraction. Polyethylene is used as the matrix material with $E^m = 3.22$ GPa, $\nu_m = 0.3$ at the room temperature. For the (10,10) armchair SWCNT as the reinforcement, it is assumed that $E_{11}^{CNT} = 600$ GPa, $E_{22}^{CNT} = 10$ GPa, $G_{12}^{CNT} = 5$ GPa, $\nu_{CNT} = 0.19$ (Cornwell and Wille 1997; Popov et al. 2000).

Through matching the elastic moduli calculated by the rule of mixture and those of obtained directly from MD simulations, the carbon nanotube efficiency parameters are extracted which are given in Table 2 relevant to both short and long SWCNT reinforcements with various values of carbon nanotube volume fraction. It is worth mentioning that for the case of shear modulus, it is assumed that $\vartheta_3 = \vartheta_2$. With the comparison between the values of longitudinal and transverse Young's moduli predicted by the rule of mixture and MD simulation, it is observed that with proper choosing of ϑ_1 and ϑ_2, the rule of mixture has an excellent capability to predict the elastic properties of nanocomposites.

The values of critical axial buckling load of composite beams reinforced by short-(10,10) SWCNT with thickness of $h = 0.1$ m and various aspect ratios and carbon nanotube volume fractions are presented in Tables 3, 4, 5, 6 corresponding to simply supported-simply supported, clamped–clamped, clamped-simply supported, and clamped-free

Table 6 Critical buckling load of nanocomposite beam reinforced by short-SWCNT with clamped-free boundary conditions ($10^6 N$)

Aspect ratio (L/h)	Carbon nanotube volume fraction (%)	Euler–Bernoulli beam theory	Timoshenko beam theory	Reddy beam theory
10	0	0.0715	0.0696	0.0696
	5	0.0845	0.0820	0.0820
	10	0.1226	0.1185	0.1185
	15	0.1844	0.1780	0.1780
	25	0.2949	0.2809	0.2809
20	0	0.0183	0.0179	0.0181
	5	0.0216	0.0214	0.0214
	10	0.0313	0.0310	0.0310
	15	0.0470	0.0466	0.0466
	25	0.0752	0.0743	0.0743
50	0	0.0029	0.0029	0.0029
	5	0.0035	0.0035	0.0035
	10	0.0050	0.0050	0.0050
	15	0.0074	0.0074	0.0074
	25	0.0121	0.0121	0.0121

Table 7 Critical buckling load of nanocomposite beam reinforced by long-SWCNT with simply supported-simply supported boundary conditions ($10^6 N$)

Aspect ratio (L/h)	Carbon nanotube volume fraction (%)	Euler–Bernoulli beam theory	Timoshenko beam theory	Reddy beam theory
10	0	0.2911	0.2830	0.2830
	5	6.1053	4.1142	4.1224
	10	9.0660	5.8485	5.8621
	15	13.8224	8.7641	8.7859
	25	22.2455	12.3440	12.3967
20	0	0.0734	0.0719	0.0723
	5	1.5258	1.3613	1.3618
	10	2.2661	1.9924	1.9933
	15	3.4559	3.0203	3.0211
	25	5.5610	4.6316	4.6342
50	0	0.0117	0.0124	0.0124
	5	0.2441	0.2401	0.2401
	10	0.3638	0.3546	0.3546
	15	0.5532	0.5405	0.5405
	25	0.8904	0.8620	0.8620

boundary conditions, respectively. The same results for composite beams reinforced by long-(10,10) SWCNT are tabulated in Tables 7, 8, 9, 10. It can be found from the results that the stiffness of nanoconposite beam reinforced with long-SWCNT is so higher than those reinforced with short-SWCNT.

Also it is seen that by incorporating the influence of transverse shear strains in Timoshenko and Reddy beam theories, the values of critical buckling load will be reduced from those of Euler–Bernoulli beam theory relevant to all carbon nanotube volume fraction specifically for the beams with lower aspect ratios. Furthermore, the difference between critical buckling loads predicted Timoshenko and Reddy beam theories is relatively more considerable corresponding to lower aspect ratios.

It can be observed from the results that an increase in the carbon nanotube volume fraction causes higher critical buckling load for both of short- and long-SWCNT reinforced composite beams, but it is more significant corresponding to the latter.

The extremely small dimensions of 1D nanostructures impose great challenges to many existing mechanical testing instruments, methodologies, and even theories. Calibration procedures in nanomechanical testing have been largely ignored; this may lead to different or even contrasting reports in the literature. Development of new

Table 8 Critical buckling load of nanocomposite beam reinforced by long-SWCNT with clamped–clamped supported boundary conditions ($10^6 N$)

Aspect ratio (L/h)	Carbon nanotube volume fraction (%)	Euler–Bernoulli beam theory	Timoshenko beam theory	Reddy beam theory
10	0	1.1411	1.1096	1.1096
	5	23.9328	16.1318	16.1639
	10	35.5387	22.9320	22.9853
	15	54.1838	34.3641	34.4495
	25	87.2024	48.4008	48.6074
20	0	0.2928	0.2861	0.2885
	5	6.0879	5.4352	5.4476
	10	9.0417	7.9497	7.9712
	15	13.7890	12.0510	12.0814
	25	22.1884	17.4028	18.5322
50	0	0.0464	0.0463	0.0463
	5	0.9740	0.9601	0.9601
	10	1.4548	1.4180	1.4180
	15	2.2122	2.1615	2.1615
	25	3.5607	3.4472	3.4472

Table 9 Critical buckling load of nanocomposite beam reinforced by long-SWCNT with clamped-simply supported boundary conditions ($10^6 N$)

Aspect ratio (L/h)	Carbon nanotube volume fraction (%)	Euler–Bernoulli beam theory	Timoshenko beam theory	Reddy beam theory
10	0	0.5834	0.5674	0.5674
	5	12.2411	8.2489	8.2654
	10	18.1773	11.7262	11.7535
	15	27.7139	17.5720	17.6157
	25	44.6022	24.7497	24.8553
20	0	0.1501	0.1466	0.1478
	5	3.1203	2.7837	2.7849
	10	4.6342	4.0744	4.0763
	15	7.0673	6.1765	6.1781
	25	11.3723	9.4716	9.4769
50	0	0.0239	0.0237	0.0237
	5	0.4994	0.4912	0.4912
	10	0.7443	0.7255	0.7255
	15	1.1318	1.1059	1.1059
	25	1.8217	1.7636	1.7636

nanomechanical testing techniques and calibration methods is greatly needed (Lin et al. 2010). With the advent of 2D nano-composite materials such as graphene, many researchs have been done in recent years (Li et al. 2005; Yang et al. 2013). For future wok, this research can be developed to 2D nanostructured reinforced composites.

7 Conclusion

In this work, buckling behavior of carbon nanotube-reinforced composite beams was investigated under four common sets of boundary conditions namely as simply supported-simply supported, clamped–clamped, clamped-simply supported, and clamped-free. Both of short- and long-SWCNT reinforcements were considered in the study based on different types of beam theory. The rule of mixture in conjunction with generalized differential quadrature method to discretize the constitutive differential equations was employed to obtain critical buckling loads of the nanocomposite beams. To select proper values of carbon nanotube efficiency parameters used in the rule of mixture, the elastic moduli relevant to both of composites with the short- and long-SWCNT reinforcements were evaluated

Table 10 Critical buckling load of nanocomposite beam reinforced by long-SWCNT with clamped-free boundary conditions ($10^6 N$)

Aspect ratio (L/h)	Carbon nanotube volume fraction (%)	Euler–Bernoulli beam theory	Timoshenko beam theory	Reddy beam theory
10	0	0.0715	0.0696	0.0696
	5	1.5001	1.0113	1.0133
	10	2.2275	1.4376	1.4409
	15	3.3962	2.1542	2.1596
	25	5.4657	3.0341	3.0471
20	0	0.0183	0.0179	0.0181
	5	0.3825	0.3415	0.3418
	10	0.5681	0.4995	0.4997
	15	0.8664	0.7572	0.7574
	25	1.3942	1.1611	1.1618
50	0	0.0029	0.0029	0.0029
	5	0.0612	0.0602	0.0602
	10	0.0912	0.0889	0.0889
	15	0.1387	0.1356	0.1356
	25	0.2233	0.2162	0.2162

using molecular dynamics simulation, the results of which were fitted with those obtained from the rule of mixture.

It was found that there are various carbon nanotube efficiency parameters corresponding to different values of carbon nanotube volume fraction. Moreover, it was observed that for higher values of carbon nanotube volume fraction, the stiffness of nanocomposite beam increases more in the case of long-SWCNT reinforcement compared to the short-SWCNT one.

References

Bal S (2010) Experimental study of mechanical and electrical properties of carbon nanofiber/epoxy composites. Mater Des 31:2406–2413

Berendsen HJC, Postma JPM, Van Gunsteren WF, DiNola A, Kaak JR (1984) Molecular dynamics with coupling to an external bath. J Chem Phys 81:3684–3690

Bi K, Chen Y, Yang J, Wang Y, Chen M (2006) Molecular dynamics simulation of thermal conductivity of single-wall carbon nanotubes. Phys Lett A 350:150–153

Cadek M, Coleman JN, Barron V, Hedicke K, Blau WJ (2002) Morphological and mechanical properties of carbon nanotube-reinforced semicrystalline and amorphous polymer composites. Appl Phys Lett 81:5123–5125

Cao G, Chen X, Xu ZH, Li X (2010) Measuring mechanical properties of micro- and nano-fibers embedded in an elastic substrate: theoretical framework and experiment. Compos B 41(1):33–41

Cornwell CF, Wille LT (1997) Elastic properties of single-walled carbon nanotubes in comparison. Solid State Commun 101:555–558

De Rosa MA, Auciello NM, Lippiello M (2008) Dynamic stability analysis and DQM for beams with variable cross-section. Mech Res Commun 35(3):187–192

Esawi AMK, Farag MM (2007) Carbon Nanotube reinforced composites: potential and current challenges. Mater Des 28:2394–2401

Frankland SJV, Harik VM, Odegard GM, Brenner DW, Gates TS (2003) Stress–strain behavior of polymer–nanotube composites from molecular dynamics simulation. Compos Sci Technol 63:1655–1661

Geng H, Rosen R, Zheng B, Shimoda H, Fleming L, Liu J et al (2002) Fabrication and properties of composites of poly (ethylene oxide) and functionalized carbon nanotubes. Adv Mater 14:1387–1390

Gong X, Liu J, Baskaran S, Voise RD, Young JS (2000) Surfactant assisted processing of carbon nanotube/polymer composites. Chem Mater 12:1049–4052

Haftchenari H, Darvizeh M, Darvizeh A, Ansari R, Sharma CB (2007) Dynamic analysis of composite cylindrical shells using differential quadrature method (DQM). Compos Struct 78(2):292–298

Hammel E, Tang X, Trampert M, Schmitt T, Mauthner K, Eder A (2004) Carbon nanofibers for composite applications. Carbon 42:1153–1158

Han Y, Elliott J (2007) Molecular dynamics simulations of the elastic properties of polymer/carbon nanotube composites. Comput Mater Sci 39:315–323

Hanasaki I, Nakatani A, Kitagawa H (2004) Molecular dynamics study of Ar flow and He flow inside carbon nanotube junction as a molecular nozzle and diffuser. Sci Technol Adv Mater 5:107–113

Haque A, Ramasetty A (2005) Theoretical study of stress transfer in carbon nanotube reinforced polymer matrix composites. Compos Struct 71:68–77

Hu YJ, Zhu YY, Cheng CJ (2009) DQM for dynamic response of fluid-saturated visco-elastic porous media. Int J Solids Struct 46(7–8):1667–1675

Iijima S (1991) Helical microtubes of graphite carbon. Nature 354:56–58

Labuschange A, Van Rensburg NFJ, Van der Merwe AJ (2009) Comparison of linear beam theories. Math Comput Model 49:20–30

Lau K (2003) Interfacial bonding characteristics of nanotube/polymer composites. Chem Phys Lett 370:399–405

Lau KT, Gu C, Hui D (2006) A critical review on nanotube and nanotube/nanoclay related polymer composite materials. Compos B 37:425–436

Li X, Gao H, Scrivens WA, Fei D, Thakur V, Sutton MA, Myrick ML (2005) Structural and mechanical characterization of

nanoclay-reinforced agarose nanocomposites. Nanotechnology 16(10):2020
Liao K, Li S (2001) Interfacial characteristics of a carbon nanotube–polystyrene composite system. Appl Phys Lett 79:4225–4227
Lin CH, Ni H, Wang X, Chang M, Chao YJ, Deka JR, Li X (2010) In situ nanomechanical characterization of single-crystalline boron nanowires by buckling. Small 6(8):927–931
Lozano K, Barrera EV (2001) Nanofiber-reinforced thermoplastic composites. I. Thermoanalytical and mechanical analyses. J Appl Polym Sci 79:125–133
Malekzadeh P, Fiouz AR (2007) Large deformation analysis of orthotropic skew plates with nonlinear rotationally restrained edges using DQM. Compos Struct 80(2):196–206
Nanorex Inc. (2005) NanoHive-1 v.1.2.0-b1. www.nanoengineer-1.com
Popov VN, Van Doren VE, Balkanski M (2000) Elastic properties of crystals of single-walled carbon nanotube. Solid State Commun 114:395–399
Pradhan SC, Murmu T (2010) Application of nonlocal elasticity and DQM in the flapwise bending vibration of a rotating nanocantilever. Phys E 42(7):1944–1949
Qian D, Dickey EC, Andrews R, Rantell T (2000) Load transfer and deformation mechanisms in carbon nanotube–polystyrene composites. Appl Phys Lett 76:2868–2870
Saffar KPA, Jamalipour N, Najafi AR, Rouhi G, Arshi AR, Fereidoon A (2008) A finite element model for estimating Young's modulus of carbon nanotube reinforced composites incorporating elastic cross-links. Int J Mech Sci 3:172–175
Schadler LS, Giannairs SC, Ajayan PM (1998) Load transfer in carbon nanotube epoxy composites. Appl Phys Lett 73:3842–3844
Sepahi O, Forouzan MR, Malekzadeh P (2010) Large deflection analysis of thermo-mechanical loaded annular FGM plates on nonlinear elastic foundation via DQM. Compos Struct 92(10):2369–2378
Shen HS (2009) Nonlinear bending of functionally graded carbon nanotube-reinforced composite plates in thermal environments. Compos Struct 91:9–19
Shokrieh MM, Rafiee R (2010) On the tensile behavior of an embedded carbon nanotube in polymer matrix with non-bonded interphase region. Compos Struct 92:647–652
Stuart SJ, Tutein AB, Harrison JA (2000) A reactive potential for hydrocarbons with intermolecular interactions. J Chem Phys 112:6472–6486
Villoria RG, Miravete A (2007) Mechanical model to evaluate the effect of the dispersion in nanocomposites. Acta Mater 55:3025–3031
Wei C, Cho K, Srivastava D (2001) Chemical bonding of polymer on carbon nanotube. In: MRS proceedings, vol 675. Cambridge University Press, pp 4–7
Xiao JR, Lopatnikov SL, Gama BA, Gillespie JW (2006) Nanomechanics on the deformation of single- and multi-walled carbon nanotube under radial pressure. Mater Sci Eng A 416:192–204
Xu X, Thwe MM, Shearwood C, Liao K (2002) Mechanical properties and interfacial characteristics of carbon nanotube-reinforced epoxy thin films. Appl Phys Lett 81:28–33
Yang Y, Rigdon W, Huang X, Li X (2013) Enhancing graphene reinforcing potential in composites by hydrogen passivation induced dispersion. Sci Rep 3:2086
Zeng QH, Yu AB, Lu GQ (2008) Multiscale modeling and simulation of polymer nanocomposites. Progress Polym Sci 33:191–269
Zhang CL, Shen HS (2006) Temperature-dependent elastic properties of single-walled carbon nanotubes: prediction from molecular dynamics simulation. Appl Phys Lett 89:081904